Microgravity Bubble Migration in Rotating Flows

J. S. Ruggles,* R. G. Cook,† and R. Cole‡
Clarkson University, Potsdam, New York

The near-free-fall environment of an orbiting space laboratory allows materials such as glassmelts to be processed in a "containerless" mode. Under such conditions, rotation of the melt, followed by thermocapillary migration of the coalesced bubbles results in a "centrifugal fining" operation for bubble removal from the melt. For this study, the NASA KC-135 environment was used to obtain experimental data on the migration of bubbles in rotating liquid fields under reduced gravity conditions. The data were compared to an analysis developed to predict the trajectory of a fluid particle in the presence of both gravitational and rotational fields at the limit of quasisteady creeping flow. The analysis predicted the experimental trajectories reasonably well considering that the bubbles were relatively large, were in close proximity to a bounding surface for a significant portion of their migration time, and were somewhat nonspherical.

Nomenclature

A = $B/(1+\epsilon^2)$, mm
a = equivalent radius of fluid particle, mm
B = $\epsilon(g/\Omega^2)$, mm
g = gravitational acceleration, m/s^2
g_0 = normal Earth gravitational acceleration, 9.81 m/s^2
R = dimensionless distance from rotation axis, = r/r_0
r = distance from rotation axis, mm
r_0 = radius of spherical shell, mm
r_∞ = asymptotic radial position, mm
Ta = Taylor number, = $a^2\Omega/\nu$, dimensionless
t = time, s
t_b = characteristic migration time, = $(\epsilon\Omega)^{-1}$, s
t_m = experimental migration time, s
t_s = spin-up time, = $r_0/(\nu\Omega)^{1/2}$, s
$(x_0,y_0,0)$ = coordinates of initial position of fluid particle (z is the rotation axis), mm
β = A/r_0, dimensionless
ϵ = $(Ta)(\Delta\rho/\rho)(2\kappa'/3)$, dimensionless
θ = angular position in equatorial plane, rad
κ = ratio of absolute viscosities, (μ_p/μ), dimensionless
κ' = $(1+\kappa)/(2+3\kappa)$, dimensionless
μ = absolute viscosity of the host liquid, kg/ms
ν = kinematic viscosity of the host liquid, m^2/s
ξ = x_0/A, dimensionless
ρ = mass density of the host liquid, kg/m^3
$\Delta\rho$ = density difference, $\rho-\rho_p$, kg/m^3
τ = dimensionless time = t/t_b
Ψ = y_0/A, dimensionless
Ω = sphere rotation rate, rad/s

Subscripts
b = bubble
p = particle
∞ = asymptotic position

Presented as Paper 88-3555 at the AIAA/ASME 1st National Fluid Dynamics Congress, Cincinnati, OH, July 25-28, 1988; received Sept. 16, 1988; revision received May 12, 1989.

*Research Assistant; currently, Patent Examiner, Patent and Trademark Office, U.S. Department Commerce, Washington, DC.
†Research Assistant; currently, Chemical Engineer, Union Carbide Corporation, South Charleston, WV.
‡Professor, Department of Chemical Engineering.

Introduction

In a free-fall environment such as that provided by the NASA space program, the absence of an effective gravitational buoyant force allows materials such as glassmelts and molten metal alloys to be levitated and processed in a containerless mode. This is advantageous to the production of materials with new and unique properties because it eliminates contamination and heterogeneous nucleation associated with contact with the container walls. The free-fall environment, however, also eliminates gravitational buoyant forces that are beneficial in producing mixing and bubble elimination. Subramanian and Cole[1] have proposed the use of rotational buoyant forces in combination with thermocapillary-induced migration to provide a form of centrifugal fining (bubble elimination). To aid in the design of space experiments associated with this phenomena, ground-based experiments have been conducted and a mathematical model developed to provide insight into the migration of small bubbles and drops in a rotating flow[2-4] Because the free-fall environment could not be simulated in our laboratories, these experiments were carried out in a liquid-filled rotating glass shell. A spherical geometry was chosen for the ground-based experiments as being reasonably representative of the shape of a containerless levitated glassmelt. Additional experiments employing the same geometry have recently been carried out in the near-free-fall environment of the NASA KC-135 aircraft. The 25- to 30-s weightless period provided by that program is of just the proper length to complement the 1-g studies. The purpose of this paper is to report the results of these studies.

Experiments

Apparatus

A NASA KC-135 aircraft specially modified for parabolic flight was employed to house the apparatus and provide a 25–30 s period of near weightlessness. The setup was made up of an aluminum frame welded to a 13-mm-thick aluminum base plate to form a cube, 0.76 m on a side.[5] Opaque acrylic plastic sheets were attached to the top and three of the sides to reduce glare from external sources. Figure 1 is a schematic diagram of the equipment located on the base plate.

The spherical test shell was formed from heat-resistant glass tubing that was softened and expanded inside a graphite mold of 70-mm inner diameter. A 5-mm-diam hole was made in the shell wall for injection of the test fluids. The shell was fused to a length of borosilicate glass tubing that was specially sealed to

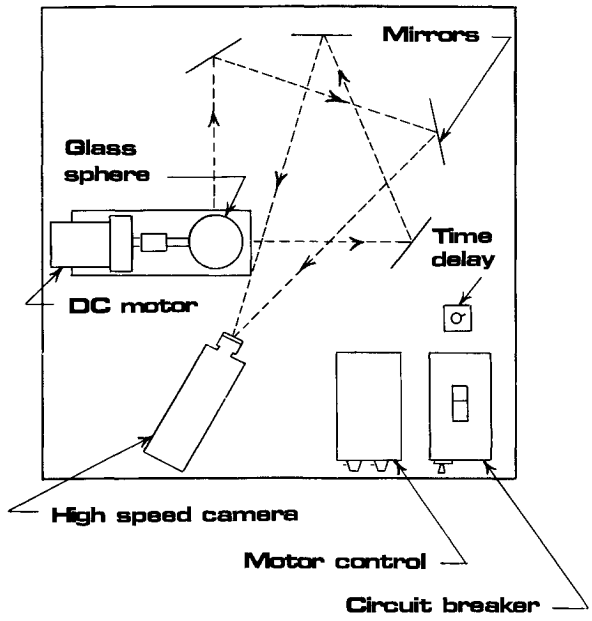

Fig. 1 Schematic diagram of experimental apparatus.

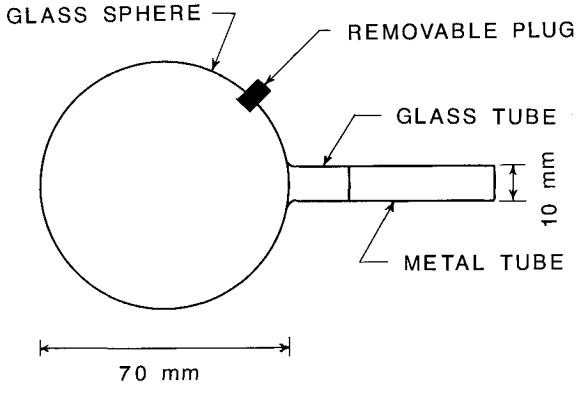

Fig. 2 Spherical glass shell.

a hollow stainless-steel tube. To reduce wobble, the assembly was rotated on its shaft while softening the fused joint. A closeup of the assembly is shown in Fig. 2 with a removable plug to seal the injection port.

The shaft was directly coupled to a Bodine dc gearmotor operated by an accompanying controller. The unit was capable of rotation rates from 0.7–31 rad/s. The motor was attached to the base plate by a slotted aluminum hold-down bracket to allow adjustment for spheres of different diameters and shaft lengths. A 0–15 s time delay relay and 15 A circuit breaker were also incorporated into the motor circuit.

A system of four 100-mm-diam optical mirrors were arranged as shown in the schematic for two simultaneous orthogonal views of the event. The mirror-mounting frames were connected to aluminum blocks bolted to the base plate.

The experiments were recorded onto ½-in. videotape using a Panasonic PK-971 color video camera and Panasonic PV-6000 portable videocassette recorder (VCR). A JVC-TM-22U color video monitor provided viewing of the recorded events. The VCR and monitor were mounted on a Plexiglas shelf inside the apparatus. Lighting was provided by a 15-W fluorescent fixture attached to the bottom of the shelf. A NASA photograph of the interior of the apparatus at the completion of the low-gravity run is shown in Fig. 3. All of the structural features and electrical systems were designed to conform to NASA KC-135 equipment specifications.[6]

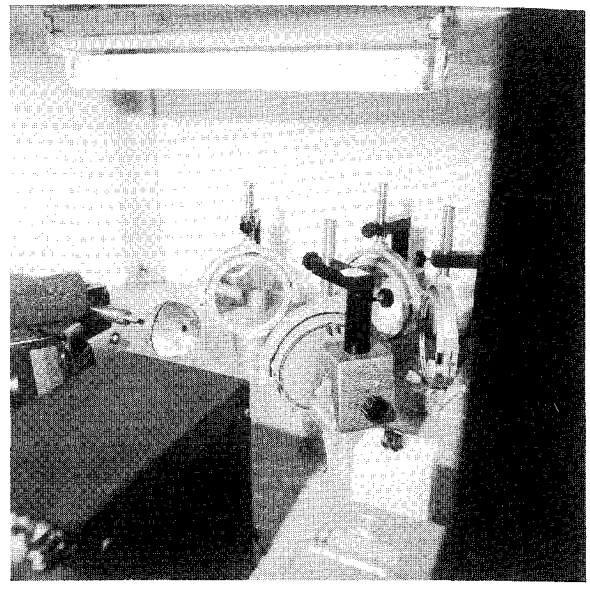

Fig. 3 Photograph of flight hardware.

Data Analysis

Analysis of the videotape was aided by the use of a Colorado Video X-Y indicator interfaced to a Zenith Z-100 microcomputer. The X-Y indicator superimposes an adjustable set of vertical and horizontal cross hairs onto the TV monitor image and generates a signal output proportional to the position of the cross hairs. The data, consisting of an identification number, time, and X and Y cross-hair positions, are converted to an appropriate form by software and stored as a data file on floppy disk. Four raw data files were stored for each run as described previously and were used with software developed specifically for this project to determine the radial bubble position at any given time, the equivalent bubble radius, the bubble shape as seen from an end view at 1/8, 3/8, 5/8, and 7/8 of the total recorded run time, and the shell rotation rate.

Because the bubble is viewed through a medium (silicone oil) having a refractive index different from that of the surroundings (air), it is necessary to correct the data for optical refraction. The correction is complicated by the curvature of the interface through which the observations are made. In this case, the interface has the shape of a sphere.

Three-dimensional optical correction equations were developed for this study[7] and require the position coordinates from two orthogonal views as input. In these experiments, the bubble remained in the equatorial plane, hence the three-dimensional equations were reduced to two-dimensions. All of the data points were corrected for optical distortion prior to use in a calculation. Finally, a computer program was developed for plotting radial position vs time and sphere revolutions, along with selected bubble shape pictures, on a commercial plotter.

Results and Discussion

The range of experimental parameters employed is shown in Table 1. The runs designated by K are the low-gravity runs and the two designated by F are the ground-based runs selected from Ref. 8 because they were conducted under similar conditions with the exception of the gravity level. The bubbles are considered to be relatively large (approximately one-third the radius of the spherical glass shell) and the viscosity of the silicone oil is 1000 and 12,500 times that of water. The rotation rates ranged from 4–10 rad/s. The range of experimental parameters employed in the low-gravity studies was limited by a number of factors.

1) The studies were initiated to obtain trajectory data for large bubbles at low rotation rates because those bubbles would not detach from the wall under normal gravity.

2) At rotation rates above 10 rad/s, the bubble motion was blurred.

3) At rotation rates much lower than 4 rad/s, there was insufficient time (with the liquid viscosities employed) for the run to be completed before the end of the low-gravity period.

The ground-based experiments are part of a more extensive study[4,8] initiated to investigate the shape, trajectory, and stability of large bubbles in rotating liquid flows and, except for the two runs shown, are not presented in this paper.

Trajectory data for the five low-gravity runs and the two normal-gravity runs are presented in Figs. 4–10 as dimensionless radial position vs both time and sphere revolutions. Additionally, the bubble shape as seen from an end view is shown at the top of each figure for approximately 1/8, 3/8, 5/8, and 7/8 of the total run time. The solid line represents the mathematical model developed by Annamalai and Cole[3] to describe the trajectory of a fluid particle in a liquid of infinite extent rotating with constant angular velocity Ω.

$$R^2 = \beta^2\{(1+\epsilon^2) + e^{-2\tau}(\xi^2+\psi^2) + 2e^{-\tau}(\xi\sin(\tau/\epsilon) + \psi\cos(\tau/\epsilon) + \epsilon[\xi\cos(\tau/\epsilon) - \psi\sin(\tau/\epsilon)]\} \quad (1)$$

In this model, secondary flows are neglected and the particle motion is assumed quasisteady. The portions of the equation that include exponential terms describe the effect of centrifugal buoyancy, whereas the trigonometric portions describe the effect of gravitational buoyancy. The latter is responsible for the oscillations that are especially evident in Fig. 5–7. The radial position, as expressed by Eq. (1), is the same when viewed from either a rotating or a stationary reference frame. The angular position when viewed from a stationary reference frame is given by[9]

$$\tan\theta = \frac{1 + [\xi\sin(\tau/\epsilon) + \psi\cos(\tau/\epsilon)]e^{-\tau}}{\epsilon + [\xi\cos(\tau/\epsilon) - \psi\sin(\tau/\epsilon)]e^{-\tau}} \quad (2)$$

In all of the trajectory figures, $t = 0$ is the time at which rotation of the sphere was initiated. Because of optical distortion, it is usually not possible to determine the exact time that the bubble leaves the wall. In these experiments, the trajectory plot has been arbitrarily initiated at the time at which the centroid of the bubble was 1.5 equivalent bubble radii distant from the wall. The coordinates of the centroid of the bubble at that time were input as the initial condition for the analysis.

Because the bubbles in this study were often not spherical, the radii reported are equivalent bubble radii and were determined experimentally at the rotation axis by measuring the

Table 1 Experimental parameters[a]

Run no.	Host liquid viscosity μ, kg/ms	Bubble radius a, mm	Gravity level, g/g_0	Final rotation rate Ω, rad/s
F14	1.01	11.3	1.0	9.76
F19	12.6	10.4	1.0	9.67
K487	1.00	13.3	0.02	4.39
K485	1.00	13.1	0.02	6.18
K407	1.00	11.0	0.02	9.30
K422	12.5	10.3	0.02	7.13
K424	12.5	10.0	0.02	9.77

[a]Host liquids used were DC-200 series silicone oils. Their density was 970 kg/m^3. The inside radius of the sphere was 35 mm.

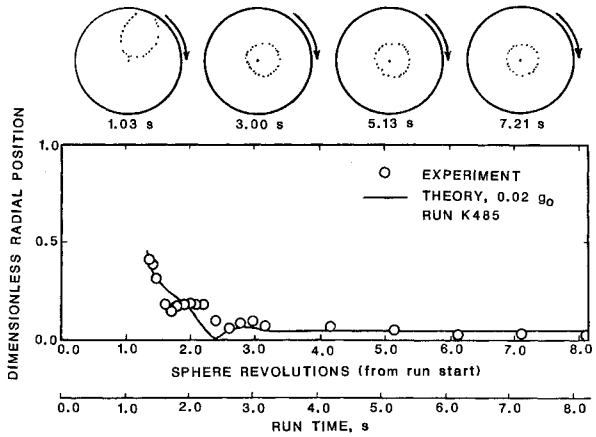

Fig. 4. Bubble migration toward the rotation axis at 0.02 g (run K485).

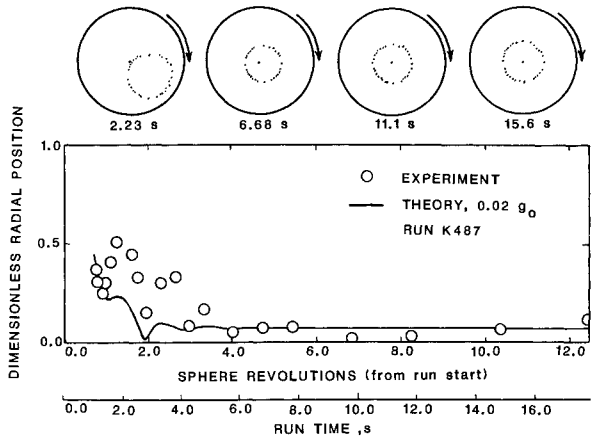

Fig. 5 Bubble migration toward the rotation axis at 0.02 g (run K487).

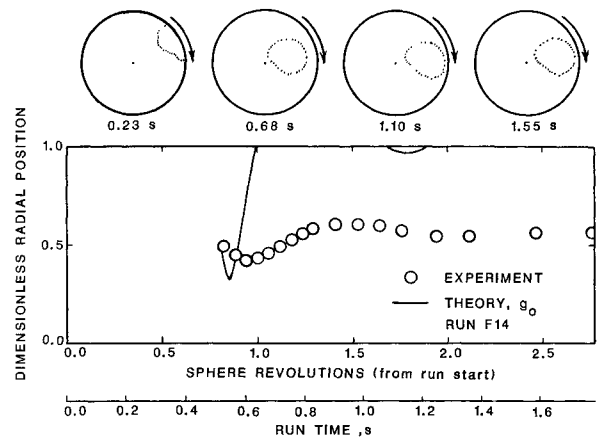

Fig. 6 Bubble migration toward the rotation axis at 1 g (run F14).

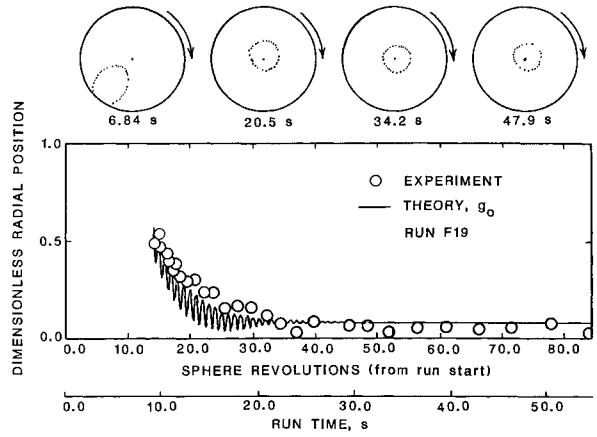

Fig. 7 Bubble migration toward the rotation axis at 1 g (run F19).

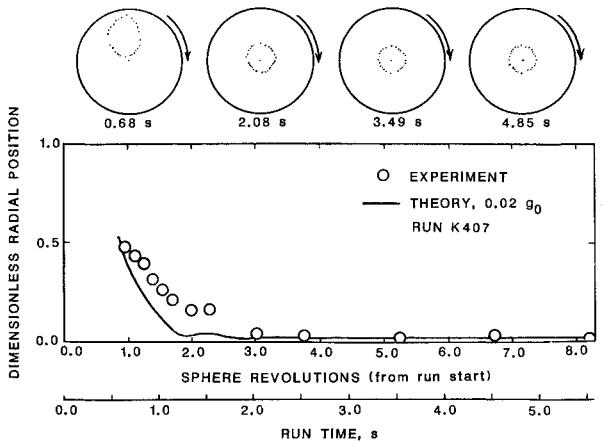

Fig. 8 Bubble migration toward the rotation axis at 0.02 *g* (run K407).

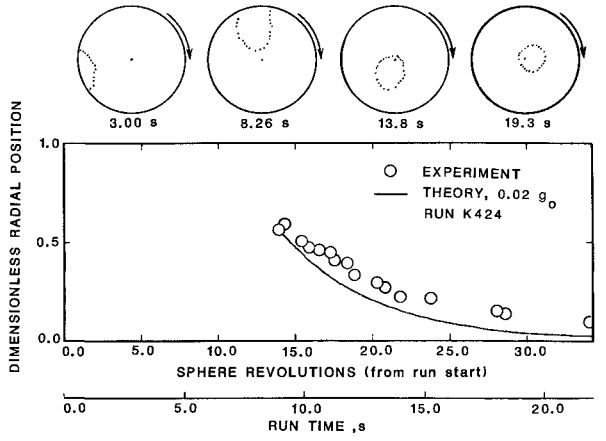

Fig. 9 Bubble migration toward the rotation axis at 0.02 *g* (run K424).

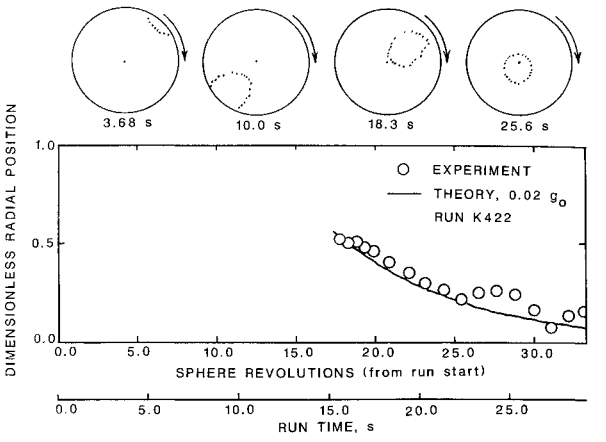

Fig. 10 Bubble migration toward the rotation axis at 0.02 *g* (run K422).

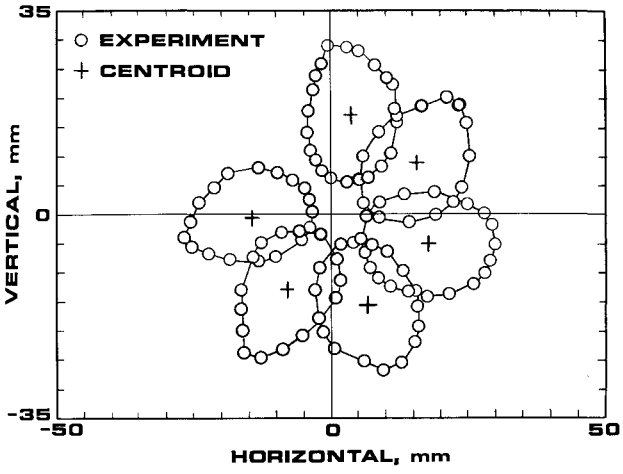

Fig. 11 Partial trajectory of a typical large bubble relative to an inertial frame of reference.

major and minor axes of the bubble from a side view and calculating the volume of an ellipsoid having the same dimensions. The equivalent bubble radius was then calculated as the radius of a sphere having the same volume as the ellipsoid. It has previously been shown[4] that the shape of a drop/bubble at the rotation axis is that of a prolate ellipsoid and is in reasonably good agreement with the analysis of Princen et al.[10]

Again, because the bubbles were often not spherical, it was necessary to devise a procedure that would allow consistent determination of the radial position of the bubble within the sphere. The method used was to divide an end view of the bubble into horizontal and vertical slices from which the centroid was determined using standard techniques. A typical trajectory illustrating the bubble shapes at various times, from which the centroids were determined, is shown in Fig. 11. At least 30 points were obtained for each shape (and corrected for optical distortion). Because of the large amount of data that had to be taken from the videotape (motion picture film in the case of the ground-based runs), shapes were usually measured only when the bubbles were at the very top and very bottom of the sphere. The bubble shapes at the top of each of the trajectory figures were determined independently as previously indicated at 1/8, 3/8, 5/8, and 7/8 of the total run time to give a qualitative indication of the bubble position and shape within the sphere. This is actual data (not just a sketch) and was also corrected for optical distortion.

In both of the ground-based runs, it is apparent that the final equilibrium position is not at the rotation axis. In fact, in run F14 (having the lower viscosity), the final radial position is approximately one-half that of the sphere radius. From Refs. 3 and 4, the asymptotic position in cylindrical polar coordinates is

$$r_\infty = \frac{g}{\Omega^2}\frac{\epsilon}{(1+\epsilon)^{1/2}} \tag{3}$$

and (relative to an inertial reference frame)

$$\theta_\infty = \tan^{-1}(1/\epsilon) \tag{4}$$

If the particle is a bubble ($\kappa = 0$, $\Delta\rho = \rho$), then $\epsilon = Ta/3$ and Eqs. (3) and (4) reduce to

$$r_\infty = \frac{g}{\Omega^2}\frac{Ta/3}{[(1+Ta/3)^2]^{1/2}} \tag{5}$$

$$\theta_\infty = \tan^{-1}(3/Ta) \tag{6}$$

The agreement with the model is reasonably good for run F19. In run F14, the bubble spends all of its lifetime in the immediate vicinity of the bounding surface and this is not accounted for in the model (which assumes a host liquid of infinite extent). It is shown in Refs. 3 and 4 that, for the quasisteady conditions under which the experiments were conducted, reasonably good agreement is obtained with the model provided that the bubble does not spend a large portion of its migration time in close proximity to the surface. Also apparent in both of the ground-based runs is the oscillatory nature of the bubble trajectory. This is a gravity-induced phenomenon and is a result of gravitational buoyancy attempting to force the bub-

Table 2 Experimental conditions

Run no.	Taylor number, *Ta*	Reynolds number, *Re*	Bubble migration time, t_m, s	Spin-up time, t_s, s	Asymptotic position, r/r_0
F14	1.20	–	>2	0.35	1.09
F19	0.08	–	21	0.10	0.08
K487	0.75	–	3.2	0.53	0.07
K485	1.03	0.44	2.6	0.44	0.05
K407	1.09	0.29	1.8	0.39	0.02
K422	0.06	0.002	>25	0.10	0.002
K424	0.08	0.003	18	0.10	0.001

ble closer to the rotation axis when it is below the axis, and farther from the rotation axis when it is above the axis.

A common characteristic of the low-gravity data is that the asymptotic position is quite close to the rotation axis. At zero gravity, the rotation axis itself is predicted by Eq. (5) to be the asymptotic position. Some oscillations are still evident in the trajectory and indeed are predicted by the model. Both the model and the data illustrate that the oscillations diminish with increasing rotation rate and increasing viscosity. Of course the oscillations also diminish with gravity level and would not exist under 0-*g* conditions. The difference between runs F14 (1 *g*) and K407 (0.02 *g*) initially appear to be great; however, the primary difference is only the asymptotic position. If not for the large influence of the wall in the 1-*g* run, it is felt that the agreement with the analytical solution would have been comparable to that in the 0.02-*g* run. Runs F19 and K424 are again similar except for the reduction in amplitude of the oscillations and the lower asymptotic postion of the bubble in the 0.02-*g* run. The agreement with analysis is reasonable in both cases. An order of magnitude increase in viscosity has in both the 1-*g* and 0.02-*g* runs increased the time required for the bubble to depart from the wall. Interestingly, there seems to be little effect of gravity on this departure time even though at lower rotation rates the bubbles would not depart from the wall in a 1-*g* environment. Control runs were in fact carried out in the KC-135 in level flight, and at the lower rotation rates the rotational buoyant force was insufficient to overcome the gravitational and surface forces holding the bubble on the surface. In the same experiment, conducted under 0.02-*g*, the bubble would eventually leave the wall and begin its inward migration. Studies of this phenomenon were limited by the short duration of the 0.02-*g* environment (25-30 s). It can be seen in runs K422 and K424 that the experiment ended before the bubble had reached its asymptotic position. In the corresponding 1-*g* run, the time required was approximately 25 s.

All of the experiments were carried out under the quasi-steady creeping-flow conditions assumed by the model. In Table 2 are listed the values of the Reynolds and Taylor numbers for each run, along with the experimental bubble migration time, the spin-up time, and the dimensionless asymptotic position as determined from Eq. (1). The Reynolds and Taylor numbers are dimensionless groups representing the ratio of inertial to viscous terms and the ratio of Coriolis to viscous terms, respectively. These are assumed to be small in the development of the model. The spin-up time indicates the time scale over which secondary flows induced by the initial sphere rotation will decay. In all cases, the experimental conditions listed in Table 1 have been chosen such that the Reynolds and Taylor numbers are small and the spin-up time is less than the bubble migration time.

Conclusions

The trajectories of bubbles having a radius as large as one-third of the sphere radius are reasonably predictable by the model of Annamalai and Cole[3] provided that the flows are quasisteady and that the bubbles are not affected by the presence of the wall. This appears to be true both in normal gravity and in low gravity. A similar statement can be made about the final asymptotic position of the migrating bubble. The amplitude of the oscillations along with the final asymptotic position diminish with increasing rotation rate, increasing viscosity, and decreasing gravity level. In the limit of zero gravity, the rotation axis becomes the asymptotic location of the bubble, and gravitationally induced oscillations vanish.

Acknowledgments

This work was supported by the NASA Division of Microgravity Science and Applications through Contract NAS8-32944 from the NASA Marshall Space Flight Center with Clarkson University. The authors gratefully appreciate the participation of Professor R. S. Subramanian in the technical discussions of this problem. We also wish to acknowledge the aid of Dr. Robert E. Shurney from the NASA Marshall Space Flight Center and the KC-135 pilots and support crew.

References

[1]Annamalai, P., Shankar, N., Cole, R., and Subramanian, R. S., "Bubble Migration Inside a Liquid Drop in a Space Laboratory," *Applied Scientific Research*, Vol. 38, 1982, pp. 179–186.

[2]Annamalai, P., Subramanian, R. S., and Cole, R., "Bubble Migration in a Rotating Liquid-Filled Sphere," *Physics of Fluids*, Vol. 25, July 1982, pp. 1121–1126.

[3]Annamalai, P. and Cole, R., "Particle Migration in Rotating Liquids," *Physics of Fluids*, Vol. 29, March 1986, pp. 647–649.

[4]Ruggles, J.S., Cook, R.G., Annamalai, P., and Cole, R., "Bubble and Drop Trajectories in Rotating Flows," *Experimental Thermal and Fluid Science,* Vol. 1, No. 3, 1988, pp. 293–301.

[5]Cook, R. G., "Interfacial Shapes and Trajectories in Rotating Flows," M. S. Thesis, Clarkson Univ., Potsdam, NY, Sept. 1984.

[6]Shurney, R. E., "Man/Systems Simulation User's Guide," NASA Marshall Space Flight Center, AL, Rept. MFSC-DOC-1263, Nov. 1985.

[7]Hayes, B. E., "A Three-Dimensional Correction for Optical Refraction," M. S. Thesis, Clarkson Univ., Potsdam, NY, May 1987.

[8]Ruggles, J. R., "The Migration of a Large Nonspherical Bubble in a Rotating Liquid," M. S. Thesis, Clarkson Univ., Potsdam, NY, Dec. 1987.

[9]Annamalai, P., "Bubble and Drop Dynamics in Rotating Liquids," Ph.D. Thesis, Clarkson Univ., Potsdam, NY, Jan. 1983.

[10]Princen, H. M., Zia, I.Y.Z., and Mason, S. G., "Measurement of Interfacial Tension from the Shape of a Rotating Drop," *Journal of Colloid Interface Science,* Vol. 23, No. 1, 1967, pp. 99–107.